Article

An Experimental Study on the Characteristics of NO$_x$ Distributions at the SNCR Inlets of a Large-Scale CFB Boiler

Jin Yan [1,2,]*[iD], Xiaofeng Lu [2], Changfei Zhang [1,3], Qianjun Li [1,3], Jinping Wang [3], Shirong Liu [4], Xiong Zheng [2] and Xuchen Fan [2]

1. College of Energy and Power Engineering, Nanjing Institute of Technology, Nanjing 211167, China; drdx1984@njit.edu.cn (C.Z.); hjliqianjun@njit.edu.cn (Q.L.)
2. Key Laboratory of Low-grade Energy Utilization Technologies and Systems, Ministry of Education of PRC, Chongqing University, Chongqing 400044, China; xfluke@cqu.edu.cn (X.L.); x.zheng@cqu.edu.cn (X.Z.); 20181001003@cqu.edu.cn (X.F.)
3. Key Laboratory of Energy Thermal Conversion and Control of Ministry of Education, Southeast University, Nanjing 210096, China; wjp@seu.edu.cn
4. Datang Wu'an Power Plant Co. Ltd., Handan 056300, China; zjb@cdt-wafd.com
* Correspondence: jinyan@njit.edu.cn; Tel.: +86-18151004185

Abstract: The unknown NO$_x$ distributions inside large-scale CFB (circulating fluidized bed) boilers have always hindered the economy of the SNCR (selective non-catalytic reduction) process. In this study, field tests were carried out on a typical 300 MW CFB boiler, where multi-level 316 L-made probe and Ecom-J2KN/Testo 350 analyzers were used to perform detailed two-dimensional distributions of flue gas composition at SNCR inlets for the first time. The penetration depth inside the horizontal flue pass was up to 7 m. The NO$_x$ distributions were analyzed in detail combining with the auxiliary test in the dilute phase zone. Key results show that the average O$_2$ concentrations in #A and #C regions were 6.52% and 0.95%, respectively. The vertical NO$_x$ distributions of #A and #C SNCR inlets were similar, showing a trend of first increasing and then decreasing with peak value all appeared at 5 m depth, while the NO$_x$ distribution of #B SNCR inlet was basically increasing. Some local areas with extremely high NO$_x$ concentration (over 2000 mg/m^3) were observed near the inclined edge of SNCR inlets, which has never been reported before. Based on this, the optimization of urea injections was conducted, which could save 15.7% of the urea solution consumption while ensuring ultra-low emission of NO$_x$.

Keywords: large-scale CFB; NO$_x$ distribution; SNCR; urea optimization

1. Introduction

In recent years, the circulating fluidized bed (CFB) technology has developed rapidly because of its advantages in fuel flexibility and load regulation [1–4]. The low-temperature combustion inside the furnace also provides sufficient benefits for de-NO$_x$ combustion [5,6] and high-efficient desulfurization [7]. Meanwhile, the operating temperature of the cyclone ranges from 800 to 950 °C, which is very suitable for the selective non-catalytic reduction (SNCR) system. The high-velocity rotation and strong turbulence intensity of flue gas promote the mixing of NO$_x$ with reduction agents. In general, the NO$_x$ emission can be limited below 100 mg/m^3 with SNCR technology [8,9]. However, with the increasingly stringent requirements of environmental protection, the conventional treatments have been difficult to meet the updated NO$_x$ emission standard (50 mg/m^3 at 6% O$_2$) [10].

Thus, various de-NO$_x$ combustion technologies emerged as the times required, including air-staging [11], improvement of cyclone efficiency [12], fluidization state specification [13], flue gas recirculation [14] and optimization of urea injection [15]. Most utility boilers could meet the ultra-low emission standards after retrofit, while the problems of high NH$_3$ escape and low NO$_x$-removal efficiency existed in a large number of power plants.

Including but not limited to CFB boiler, many scholars focused on the mechanism of SNCR reactions to improve de-NOx efficiency. Taking the cyclone of a 660 MW CFB boiler as the object, Kang et al. [16] obtained a simplified 18-element mechanism using CHEMKIN software; the optimal temperature window was then proposed by combining with CFD simulation. When the gas temperature was not sufficient, the NO_x-removal efficiency could also be improved to a certain extent by increasing the ratio of ammonia to nitrogen (NSR). Yao et al. [17] compared the effect of CO and CH_4 on NO reduction in a tubular reactor with simulated flue gas. At low temperatures, the additive of C_3H_8 was the most efficient in enhancing SNCR process. At pressurized oxy-combustion condition, kinetic modeling was carried out by Rahman et al. [18] to simulate and optimize the SNCR process. The de-NO_x efficiency increased as the pressure increased from 1 to 10 atm. At high pressure, the generation of NNH showed to be the most promoting reaction. Świeboda et al. [19] reviewed the application of SNCR technology in pulverized coal-fired boilers and pointed out that the measurement of exhaust gas parameters was the most direct validation for SNCR optimization.

It is generally believed that significant non-uniform input parameters exist in large-scale CFB boilers, including primary air and secondary air [20,21], fuel particle dispersion [22], coal feed distribution [23,24], recirculating ash and heat absorption deviation in multi-parallel loops. Therefore, the flue gas composition at furnace outlets should also be uneven. Generally speaking, the smaller the uniformity deviation of NSR distribution is, the higher NO_x-removal efficiency is. On the contrary, the worse the mixing of urea solution with NO_x will be, which not only affects the NO_x-removal efficiency, but also may generate a sharp increase of NH_3 escape in some local areas. Therefore, it is particularly important to obtain the actual NO_x distributions at SNCR inlets for accurate urea injections. In the selective catalytic reduction (SCR) system commonly adopted in pulverized coal boiler, the non-uniform NO_x distribution and flow field can be directly calculated [25] or even measured [26] due to low solid concentration and gas temperature. For example, Liu et al. [27] proposed a prediction-assisted feed-forward to enhance outlet NO_x control; 22 key operating parameters were considered in the MLR (multi-layer perception) method and the original dynamic NO_x emission was predicted successfully.

However, due to stronger thermal inertia and harsher in-furnace processes, it is difficult to dynamically monitor the NO_x distributions at the SNCR inlets of CFB boilers. Thus, on-site measurement shows to be the key means to solve this problem. Niklasson et al. [28] performed on-line measurements with zirconia cell probe successfully. Hartge et al. [29] designed novel probes to measure flue gas at various levels inside a 235 MW CFB boiler. The maximum penetration depth reached 3 m. A wall region with a thickness of 0.5 m was observed in the test, and the non-uniformity of gas composition in front and rear walls was attributed to fuel distribution. With a self-made sampling device system, the authors once measured the gas along the horizontal direction of secondary air ports with a maximum sampling depth up to 4 m [30]. The oxygen distribution and jet penetration at the lower part of the furnace were basically predicted.

The above literature indicates that many studies are available concerning the SCR process or the reaction mechanism during SNCR process, but few are related to the non-uniformity of NO_x concentration at the SNCR entrance of CFB boilers. In particular, relevant field tests have rarely been reported. Nonetheless, the accumulation of the studies in [28,29,31] inspires the scholars to further explore more detailed NO_x distributions in large-scale CFB boilers through the field test approach. Thus, the present contribution reports a preliminary investigation into a typical 300 MW CFB boiler, focusing on measuring the characteristics of NO_x distributions at the SNCR inlets. By comparison with the auxiliary test in the dilute phase, the non-uniformity of NO_x distribution was analyzed in detail. In addition, local regions with ultra-high NO_x concentration were captured at the inclined edge of the SNCR inlets for the first time. Based on the measured NO_x distributions, the regulation of precise urea injections was proposed, which could save 15.7% of the urea consumption while ensuring ultra-low emission of NO_x. It is the first time to achieve

the sampling depth up to 7 m, and the detailed two-dimensional distributions of NO_x concentration were obtained. The results provide the lasting source for the improvement of CFB combustor model, and a direct reference for the prediction of NO_x distribution at SNCR entrance to enhance de-NO_x efficiency in large-scale CFB boilers.

2. Experimental Section

2.1. The 300 MW Utility CFB Boiler

As shown in Figure 1, the tested 300 MW CFB boiler has single furnace, single air distributor and three steam-cooled cyclones, labeled A–C from the left wall to the right wall. The cross-sectional area of the furnace is 28.3×9.8 m^2. Circulating ash return from the rear wall through six seal loops to improve the uniformity of bed temperature distribution. Eight coal feed ports are arranged on the front wall, the primary air enters the windbox from two sides and the secondary air is blown into the chamber through the high and low levels at the front and rear walls. Eighteen L-shape platen heat exchangers consist of three different types with the same numbers, namely intermediate temperature superheater (ITS), high temperature superheaters (THS) and high temperature reheaters (HTR). They protrude into the furnace at two heights from the front wall. Two water-cooled evaporation walls are arranged on the rear wall. The SNCR system with urea solution injections is installed on each side of the three cyclone inlets. The main design parameters of this boiler are exhibited in Table 1.
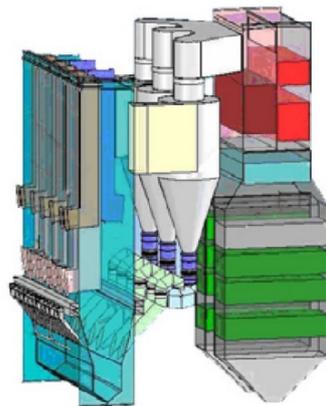
Figure 1. Schematic diagram of the 300 MW CFB boiler.

Table 1. Design parameters of the 300 MW CFB boiler.

Item	Unit	Value (BMCR)
Superheat steam flow rate	t/h	1100
Superheated steam pressure	MPa	17.4
Superheated steam temperature	°C	541
Reheat steam pressure	MPa	3.87
Reheat steam temperature	°C	541
Water feed temperature	°C	282

2.2. Measurement Port Arrangement and Test Procedure

As illustrated in Figure 2, the vertical measurement ports at SNCR inlets of the three cyclones were all installed in the middle of the roof of the horizontal flue pass and were about 700 mm before the injection of the urea spray guns. The sampling probe was composed of four 316 L stainless steel tubes with sectional size of 28 mm $\times$ 6 mm and a length of 2200 mm; all tubes were connected by threads. With such a long probe, complex chemical reactions could occur at the same time due to the absence of water-cooling, and all the deviations must be related to the probe length. In our previous study [30], the flue gas could continue to react with C-bearing species of the tube walls, but the S-bearing species

did not change significantly. Thus, the measurement errors of O_2 and CO with a 2.2 m, 316 L probe were -4% and 8.6%, and the concentrations of SO_2 and NO_x had no obvious changes. However, the deviations corresponding to longer probes could not increase linearly to a certain extent as it was also affected by the absolute value of oxygen concentration and gas temperature. In fact, the measurement error of O_2 should be obviously higher than proposed, while the measurement errors of NO_x and CO were hard to be clarified at this stage, as the potential reactions of NO, NO_2 and CO with O_2 could also cause major changes. The authors hoped to reduce the measurement errors within the scope of existing cognition. Thus, the previous obtained measurement errors were adopted, and the same relative corrections were applied to all the corresponding measured data.
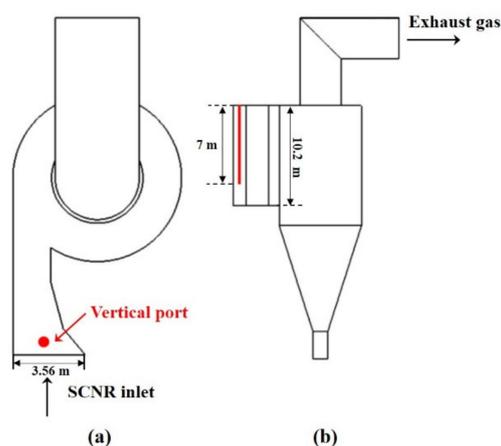
Figure 2. Positions of the vertical measurement ports of the three SNCR inlets: (**a**) top view; and (**b**) side view.

The analysis system was composed of the above-mentioned probe, filter device, vacuum pump, three-way valve and gas analyzers. Two gas analyzers were used in this test, as detailed in Table 2. The Ecom-J2KN type analyzer was for routine use, while the Testo 350 type analyzer would be used in the areas with odd values or large concentration gradients as a check. According to our experience of on-site tests, the gas composition would still show sinusoidal fluctuation under stable loads [32,33], so at least two groups of peak/valley values of flue gas should be recorded.

Table 2. Information of the two gas analyzers used in the test.

Item	Sensor Type	Range	Precision (Based on Measured Values)
Ecom-J2KN type analyzer			
O_2	Electrochemical	0–21%	0.2%
CO[1]	Electrochemical	0–10,000 ppm	5%
NO	Electrochemical	0–5000 ppm	5%
NO_2	Electrochemical	0–1000 ppm	5%
SO_2	Electrochemical	0–5000 ppm	5%
Testo 350 type analyzer			
O_2	Electrochemical	0–25%	0.8%
CO[1]	Electrochemical	0–10,000 ppm	10%
NO	Electrochemical	0–4000 ppm	5%
NO_2	Electrochemical	0–500 ppm	5%
SO_2[2]	Electrochemical	0–5000 ppm	5%

[1] CO sensors contain H_2 compensation. [2] Anti-interference of CO up to 10,000 ppm.

As the height of the horizontal flue pass was 10 m and the ash deposition layer at the bottom was about 2–3 m, the maximum penetration depth of 7 m could basically cover

the flow area of the SNCR inlets. Meanwhile, to figure out the relationship of flue gas composition between the SNCR inlets and the dilute phase zone, two measurement ports were installed at 20.6 m above the distributor in the corresponding area of cyclone #A, as shown in Figure 3. The maximum penetration depth of each measurement port was about 5 m, so the combustion and pollutant distribution in the whole depth direction of the furnace could be obtained. The above two tests were carried out at the same time to ensure comparability.
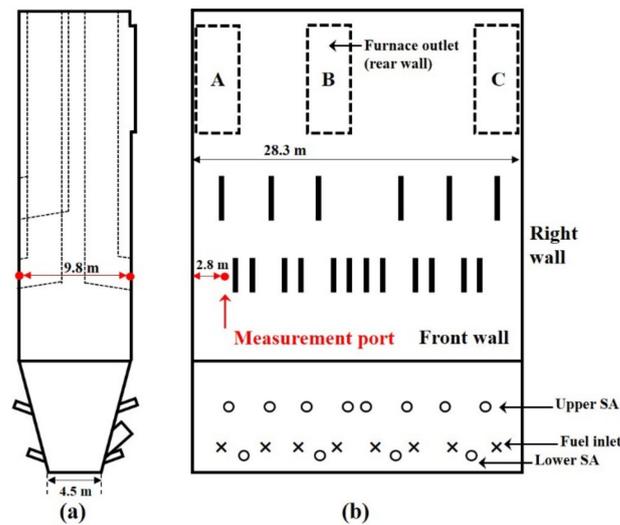
Figure 3. Positions of the horizontal measurement ports in the dilute phase: (**a**) view from the side wall; and (**b**) view from the front wall.

Each horizontal measurement port adopted the urea spray guns at the straight edge of the horizontal flue pass, i.e., #1–#6 shown in Figure 4. Because the inner side of the cyclone inlet was inclined, the horizontal measurement could not characterize the cross-sectional distribution precisely, so the #7–#10 spray guns were not adopted as measurement ports. The distances between these urea injections and the roof of the horizontal flue pass were 1.86, 3.32, 3.9, 6.55, 7.05 and 7.65 m. respectively. The width of the horizontal flue pass corresponding to the spray guns was about 2.2 m, so the sampling probe was composed of two 316 L stainless steel tubes. To avoid the influence of adjacent urea injections, the valves of the #7–#10 spray guns at the inclined edge were closed in turn during the test inside each spray gun.

Spray No.	h/m
#1, #7	1.86
#5	3.32
#2, #8	3.90
#3, #9	6.55
#6	7.05
#4, #10	8.35
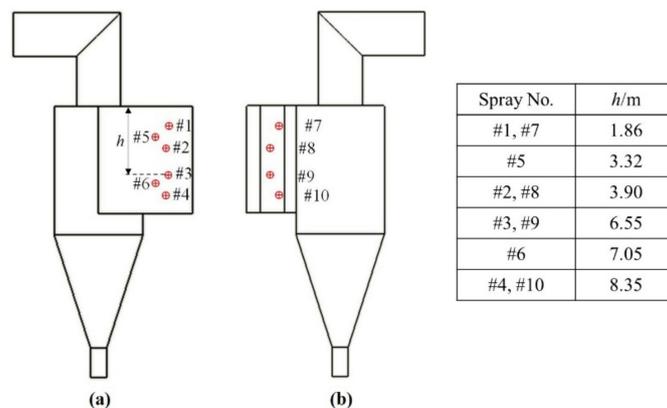
Figure 4. Detailed positions of the urea pray guns/horizontal measurement ports at SNCR inlets: (**a**) view from the straight edge; and (**b**) view from the inclined edge.

2.3. Working Condition Arrangement

Three-day stable load periods were applied to keep the unit load and operating parameters relatively stable, during which the trial test, regular test and repetitive test were conducted. The main operating conditions corresponding to each measurement are listed in Tables 3 and 4, where the bed temperatures refer to those in the corresponding area of each circulating loop. The ultimate and proximate analysis of the experimental coal is shown in Table 5.

Table 3. Main operating parameters of the boiler during the tests of the dilute phase and the vertical measurement ports at SNCR inlets (Y-vertical direction)

Item	Unit	Dilute Phase	#A-Y	#B-Y	#C-Y
Load	MW	270	270	266	268
Coal feed rate	t/h	151	151	146	150
PA flow rate	kNm^3/h	507	507	487	499
SA flow rate	kNm^3/h	310	310	299	302
Bed pressure	kPa	7.41	7.43	7.68	7.69
Bed temperature	°C	918	920	930	937
Cyclone inlet temperature	°C	932	931	984	975
Cyclone outlet temperature	°C	882	882	942	933
Economizer O$_2$	Vol.-%	3.93	3.93	4.17	4.06

Table 4. Main operating parameters of the boiler during the tests of the horizontal measurement ports at SNCR inlets (X-horizontal direction).

Item	Unit	#A-X	#B-X	#C-X
Load	MW	280	279	264
Coal feed rate	t/h	170	162	136
PA flow rate	kNm^3/h	532	539	458
SA flow rate	kNm^3/h	319	318	287
Bed pressure	kPa	8.12	8.21	7.54
Bed temperature	°C	936	955	933
Cyclone inlet temperature	°C	932	962	952
Cyclone outlet temperature	°C	898	914	940
O$_2$	Vol.-%	4.26	4.15	3.78

Table 5. Proximate and ultimate analysis of the feeding coal during the tests.

Coal	Value
Proximate analysis (wt%, air dry basis)	
Ash	42.33
Fixed carbon	49.22
Moisture	8.8
Volatiles	8.45
Lower heating value (MJ/kg)	16.31
Ultimate analysis (wt%, air dry basis)	
C	52.28
H	2.69
O	1.51
N	0.52
S$_{total}$	0.67

3. Results and Discussion

3.1. Vertical Distributions of Flue Gas Composition at the SNCR Inlets

As mentioned above, to exclude the influence of accidental factors, several tests were conducted on each vertical or horizontal measurement port of the SNCR inlet. Therefore,

the typical distribution characteristics with repeatability are presented in the following results.

3.1.1. Vertical Distributions of Flue Gas Composition at #A SNCR Inlet

The vertical distributions of flue gas composition at #A horizontal flue pass is exhibited in Figure 5. During this test, it was confirmed that, when the penetration depth of the probe exceeded 7.5 m, it gradually reached the ash deposition layer. Along vertical direction, the oxygen concentration gradually decreased from 2.7% to 0.37%, and the corresponding CO concentration increased from less than 100 to 1800 mg/m^3, indicating that the lower part of the SNCR entrance was in an obvious reducing condition. This should be due to the uneven distribution of fuel and air in the corresponding dense phase zone. On the other hand, the vertical distributions of SO_2 and NO_x were shown to be parabolic, and the peak values all appeared at the sampling depth of 5 m. As in-furnace desulfurization was not adopted, it is believed that this distribution reflected the actual fuel distribution at the lower part of the furnace in the depth direction.
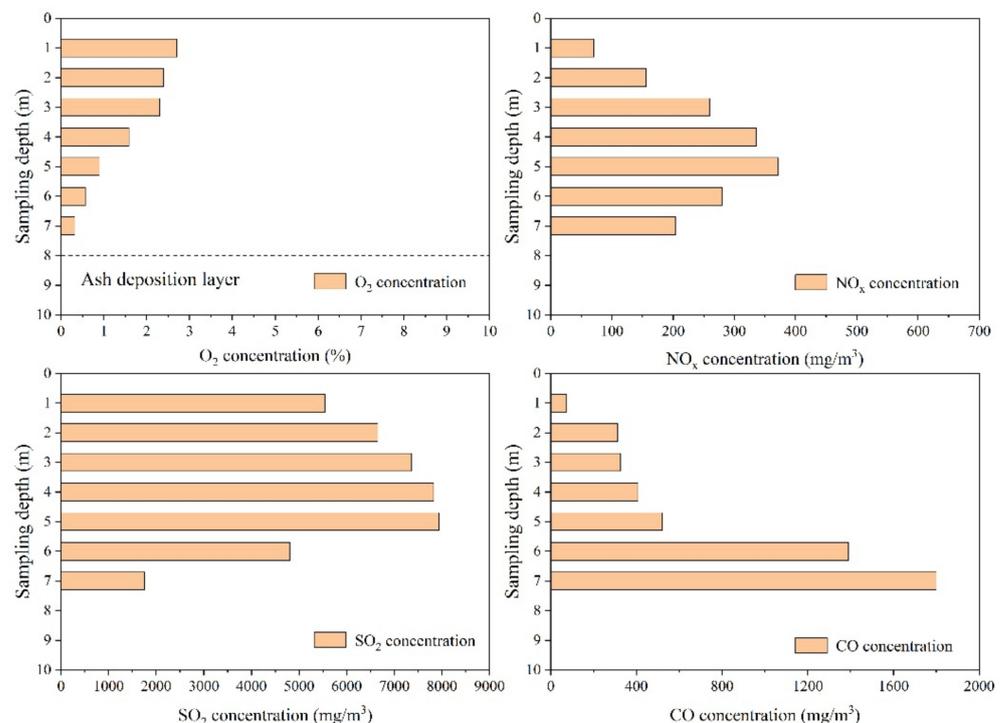
Figure 5. Vertical distributions of flue gas composition at the #A SNCR inlet.

To confirm this conjecture, Figure 6 illustrates the distribution of flue gas composition along the depth direction of the measurement port in dilute phase. It can be seen that the distribution trend of O_2 and CO concentrations was the same as that in #A SNCR inlet. Higher O_2 content was observed near the front wall. while higher CO concentration appeared near the rear wall. This indicated that the flue gas in the upper part of the horizontal flue pass mainly came from that in the front wall of the dilute phase zone; the bottom part (except the ash deposition layer) was mainly affected by the flue gas near the rear wall; and the middle part should be affected by the flue gas in the central zone of the furnace. In addition, the NO_x concentration along furnace depth also presented a parabolic distribution with an average value of about 174 mg/m^3, while the NO_x concentration at SNCR inlet reached 240 mg/m^3 with higher O_2 content, indicating that the mixing of gases played a dominant role in promoting further combustion in the upper furnace. Judged from the changes of SO_2 distribution, it was believed that combustion was mainly concentrated in the central part of the furnace, and the corresponding value increased from 6220 to 7937 mg/m^3 until the SNCR inlet.
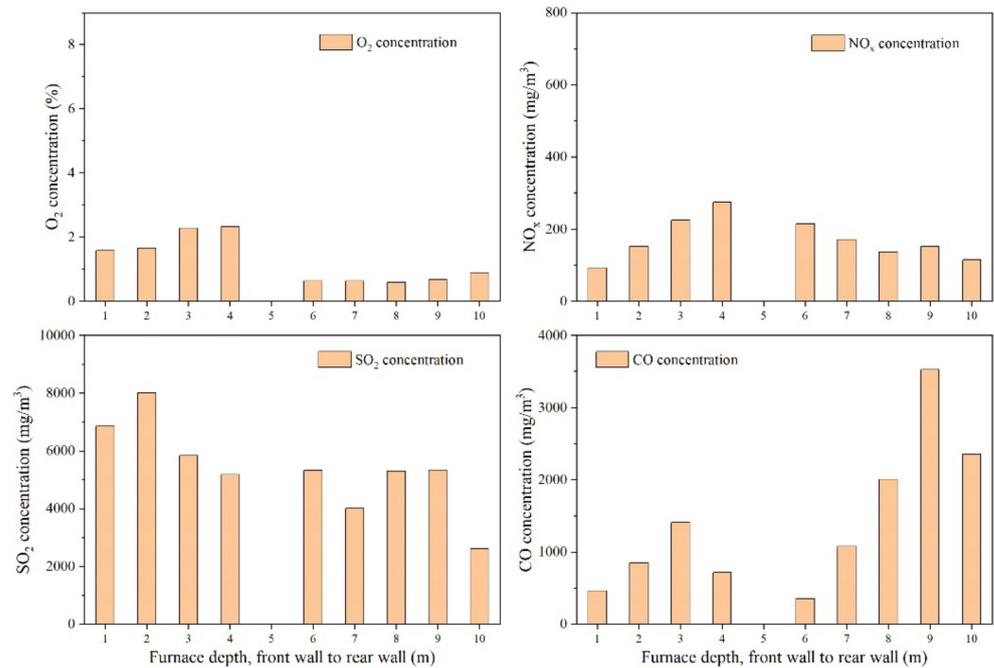
Figure 6. Horizontal distributions of flue gas composition at the dilute phase zone corresponding to the #A SNCR inlet.

3.1.2. Vertical Distributions of Flue Gas Composition at #B SNCR Inlet

The vertical distributions of flue gas composition at #B SNCR inlet is exhibited in Figure 7. The O_2 content gradually decreased along vertical direction, with the same distribution trend as that in the #A SNCR inlet. However, all the measured O_2 concentrations were over 4.69%, and the maximum value was up to 8.88%. Thus, the CO concentration remained at a very low level. To analyze this combustion difference, the coal feed distribution during the test is illustrated in Figure 8. Although some variation was obviously unavoidable, it was significant that mass flows were always the highest through feed lines #1 and #8 and lower through the middle ones. This extremely uneven coal feed distribution must be limited by the primary air distribution along furnace width, so as to provide more uniform bed temperatures. Before the test, the blast caps and secondary air nozzles were optimized to introduce more uniform air, thus it was reasonable that O_2 content in the middle part of the furnace was higher. Different from the #A SNCR inlet, the vertical distributions of NO_x and SO_2 at the #B SNCR inlet showed an increasing trend. Although the corresponding dilute phase zone was not measured, it could be judged from the above analysis that the combustion share of the coal should be higher near the rear wall. In this boiler, the coal was introduced into the furnace through seeding coal air, so the coal distribution over the bed was strongly affected by the initial momentum of fuel particles. Less coal could be thrown farther under the action of similar seeding air volume. In addition, the average SO_2 concentration was only 1772 mg/m^3, the strong oxidizing condition in the middle part could promote the generation and conversion of NO_x [34,35]. Thus, the average NO_x concentration reached 270 mg/m^3, which was higher than the measured value at #A SNCR inlet.
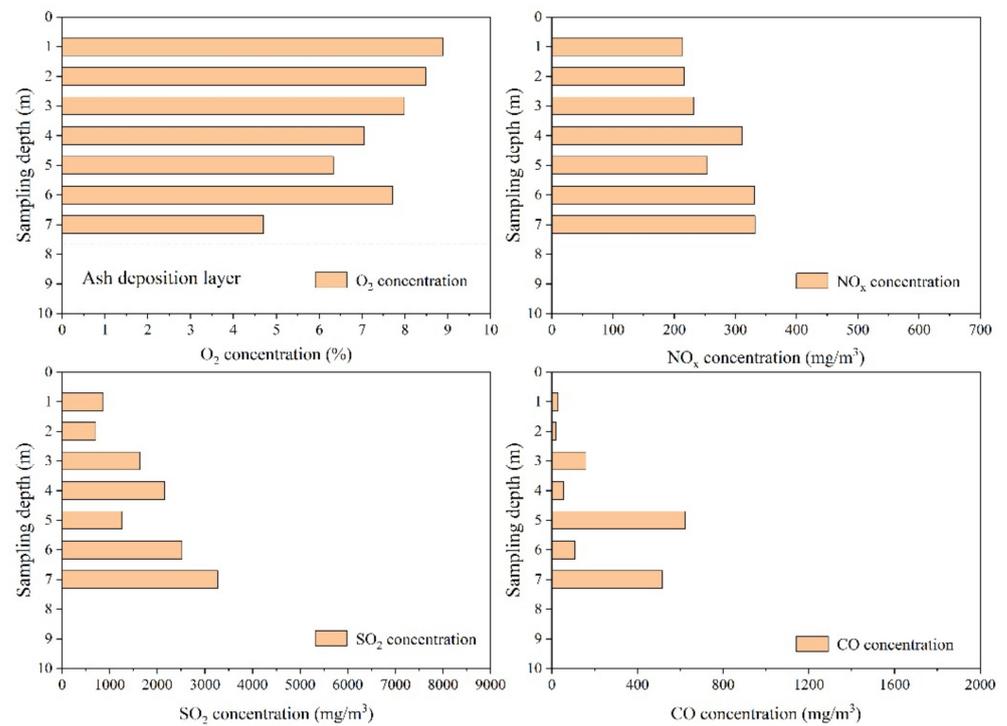
Figure 7. Vertical distributions of flue gas composition at the #B SNCR inlet.
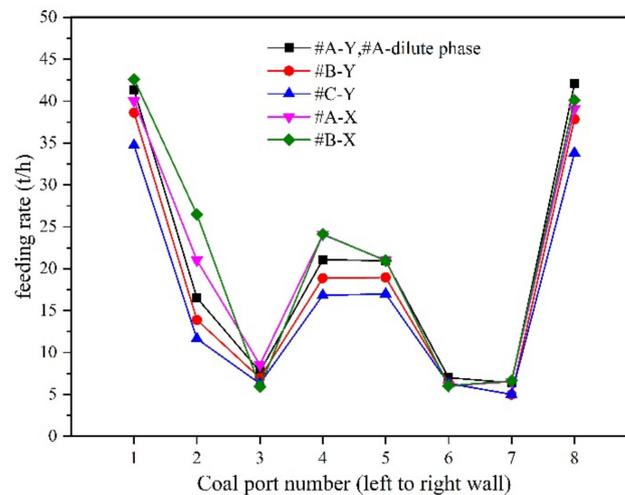
Figure 8. Fuel distributions during the measurement of at different ports.

3.1.3. Vertical Distributions of Flue Gas Composition at #C SNCR Inlet

The vertical distributions of flue gas composition at #C SNCR inlet is exhibited in Figure 9. The O_2 concentration presented a parabolic distribution, and the peak value appeared at 3 m away from the roof. The distribution of NO_x concentration was similar to that at #A SNCR inlet, and the maximum value also existed at the depth of 5 m. However, the measured value was more than 650 mg/m^3, which was far greater than the average NO_x concentration along vertical direction. After repeated tests, the accuracy of this measurement result was confirmed. This should be due to the intense combustion of feeding coal in the central part of the furnace corresponding to the #C SNCR inlet, and this influence lasted until the furnace outlet. In any case, it must be related to the initial coal distribution over the bed in the depth direction. Moreover, the SO_2 distribution was highly consistent with the NO_x distribution, which also confirmed this judgment.
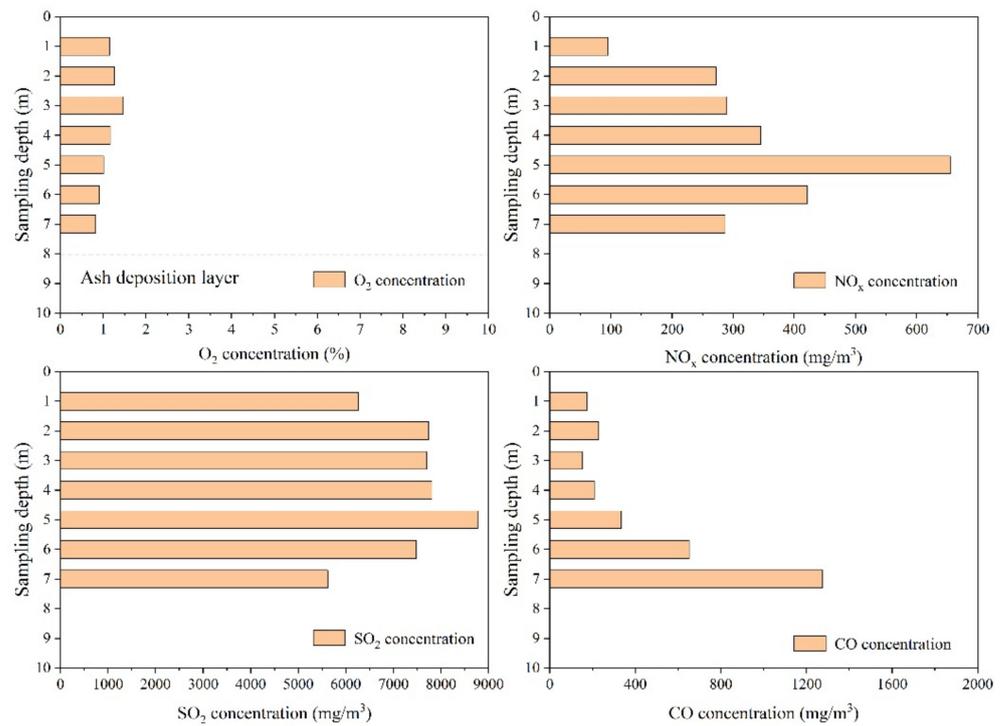
Figure 9. Vertical distributions of flue gas composition at the #C SNCR inlet.

3.2. Horizontal NO_x Distributions at the Cross Section of the SNCR Inlets

It is difficult to describe the distribution characteristics of flue gas composition only in the vertical direction of the horizontal flue duct. Therefore, it is necessary to draw a complete NO_x distribution by combining with the horizontal sampling at each height, so as to provide more powerful reference for accurate urea injections. During the measurement, part of the spray guns cannot be inserted due to the obstruction of steel frame, but we tried our best to obtain the NO_x distributions of the whole cross sections.

The horizontal distributions of NO_x concentration at #A and #C SNCR inlets are exhibited in Figure 10. For the #C SNCR inlet, only the measurements of #5 and #6 spray guns were accessible due to the obstruction of the furnace layout. However, three interesting phenomena can be summarized: (1) The NO_x concentrations in the horizontal direction of the two SNCR inlets were all maintained within 200–300 mg/m^3 except the #3 spray gun of #A SNCR inlet, and the peak value of NO_x concentration also appeared just near the #3 height. (2) No local regions with low NO_x concentration due to denitration reaction were observed. This provided a better prerequisite for optimization of accurate urea injections. (3) For the measured values at the #3 urea spray gun, the NO_x distribution had no changes after repeated tests. Along the horizontal direction, the NO_x concentration fluctuated and suddenly increased from 309 to 2890 mg/m^3 after 1200 mm depth, and finally fell back to about 785 mg/m^3 near the inclined wall.
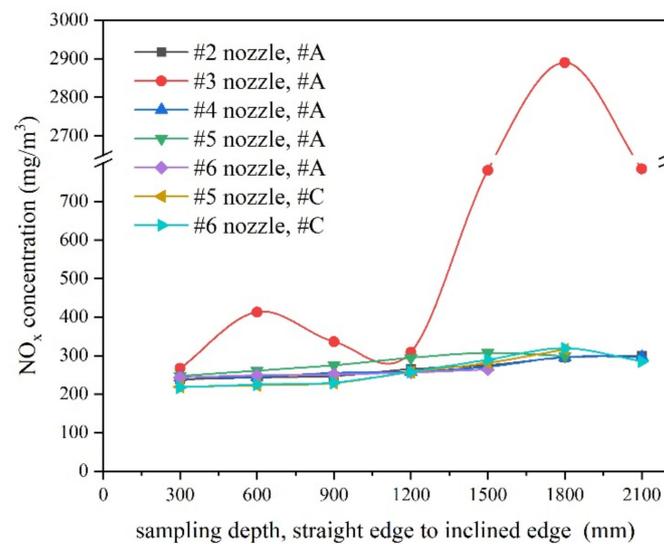
Figure 10. Horizontal distributions of NO_x concentration at the different heights of the #A and #C SNCR inlets.

The horizontal distributions of NO_x concentration at #B SNCR inlet is exhibited in Figure 11, where the position with the highest value appeared at the height of #6 urea spray gun, i.e., the bottom part of the horizontal flue pass. This is also consistent with the distribution trend shown in Figure 7. Moreover, the NO_x concentration at the height of #6 urea spray gun increased sharply from 478 to 2258 mg/m^3 after 1200 mm depth. In fact, it is difficult to explain this distribution characteristics, and such a high NO_x concentration has never been reported in the previous numerical simulations. Therefore, the authors believe that the long-term existence of high NO_x concentration in local area should be related to the following reasons: (1) local extremely uneven gas–solid flow and the subsequent devolatilization process during actual boiler operation; (2) the impact and accumulation of particles, together with unstable flow field [36] may occur near the inclined edge of the SNCR inlet, so as to increase the probability of high NO_x concentration in this region; and (3) complex chemical reactions in the hot probe, such as oxidation reactions of carbonous dust or hydrocarbon gases and competitive reactions of $NO/NO_2/CO$ when O_2 was present. This factor was unverified but existed potentially, as, when the probe was immediately moved to another measurement depth, the NO_x value decreased randomly. After turning back, the NO_x value turned to rebound again. These ultra-high concentrations of NO_x could form at the furnace outlet or in the dilute phase zone but were not captured by this test. For the #C SNCR inlet, only the measurement ports of #5 and #6 spray guns were accessible due to the obstruction of the furnace layout. Thus, the corresponding results are not exhibited in this paper because of the lack of representativeness.
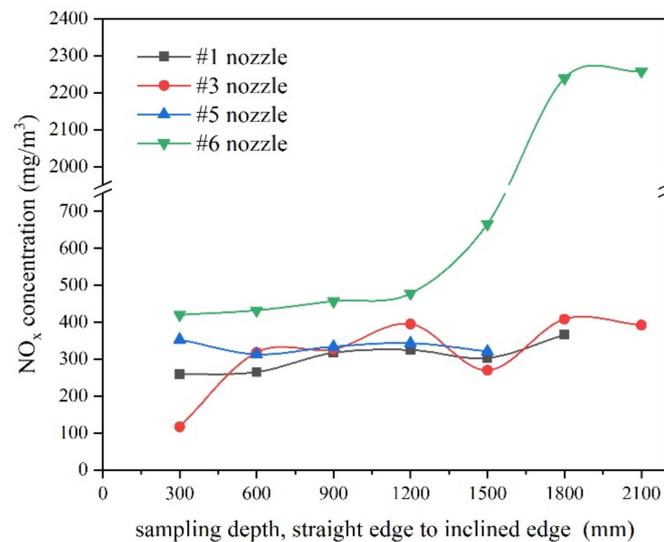
Figure 11. Horizontal distributions of NO$_x$ concentration at the different heights of the #B SNCR inlet.

3.3. Optimization of Urea Injections Based on Uneven NO$_x$ Distributions

To save urea consumption, it is necessary to obtain the NO$_x$ flux distribution of the cross section. At present, although detailed distributions of NO$_x$ concentration at the three SNCR inlets were obtained, the overall velocity field of flue gas was definitely non-uniform. According to the simulation results of Wang et al. [37], the composition and flow rate had great influence on the urea demand. Therefore, only the preliminary optimization of the flow rate in each urea spray gun was carried out. Before the optimization, the valves of all the spray gun were full open, and the flow rate of urea solution at each SNCR inlet was the same. Meanwhile, the NH$_3$ escape detected from the tail flue pass was 8.39 ppm, indicating that obvious excessive injection of urea solution was conducted in some local area.

The optimization process was divided into two steps. Firstly, the NO$_x$ concentrations were shown to be the highest in the middle section of #A and #C SNCR inlets based on the vertical measurement results. Thus, the valve openings of #2, #3, #8 and #9 spray guns were kept unchanged and the others were gradually reduced. The NO$_x$ concentration at the roof of #B SNCR inlet was the lowest, so the valve opening of #4 and #10 spray guns were kept unchanged and the others were reduced accordingly. Judged from the horizontal measured results, the local area with extremely high NO$_x$ concentration just existed at the height where the overall horizontal NO$_x$ concentration was high, so the adjustment of the inner and outer urea spray guns was consistent. Secondly, the flow rate of urea solution in the main pipe was slowly reduced in the same proportion, while the stack emission of NO$_x$ was detected at the same time. Eventually, the main operating parameters of SNCR process before and after the urea optimization are exhibited in Table 6, where the consumption of urea solution was reduced by 15.7% under the condition that the NO$_x$ stack emission was still limited below 50 mg/m^3.

Table 6. Main operating parameters of SNCR process during urea optimization.

Item	Unit	Before Optimization	After Optimization
Urea solution flowrate in #A	m^3/h	2.800	2.535
Urea solution flowrate in #B	m^3/h	2.694	1.982
Urea solution flowrate in #C	m^3/h	2.601	2.307
NH$_3$ escape	ppm	8.39	/
Stack NO$_x$ emission	mg/m^3	44.93	47.49
O$_2$	%	6.29	6.06

It should also be noted that the highest NO_x position of #A and #C SNCR inlets appeared at 5 m from the roof, which was just in the middle of #2 (#8) and #3 (#9) spray guns. Therefore, future work should be focused on the optimization of the position and injection characteristics of the spray gun and the investigation of initial distribution of fuel particles over the bed, so as to further improve the NO_x-removal efficiency during SNCR process.

4. Conclusions

In this study, field tests with deep penetration sampling were conducted on a typical large-scale CFB boiler. The horizontal and vertical distributions of flue gas composition at each SNCR inlet was successfully obtained, and the differences of NO_x concentration were analyzed in detail combined with air/coal distribution as well as one auxiliary test in dilute phase zone. Although some horizontal ports were inaccessible due to limitation of site layout, the measurements provided a complete picture of the NO_x distribution characteristics in a large utility CFB boiler for the first time.

The vertical NO_x distribution at SNCR inlet was basically consistent with that in the dilute phase zone, which depended mainly on the initial fuel dispersion along depth direction. In addition, the vertical NO_x concentration at the SNCR inlet on both sides presented a parabolic distribution but increased along height direction in the middle one. Particularly, some local areas with extremely high NO_x concentration (over 2000 mg/m^3) were captured near the inclined edge of SNCR inlets, which might be related to the potential reactions in tubes or local uneven combustion and is worthy of further study.

As a practical conclusion, the preliminary regulation of precise urea injection could save 15.7% of urea solution consumption based on the obtained two-dimensional NO_x distributions. Follow-up work should be focused on three aspects: (1) the initial distribution of fuel particles over the bed or even without bed materials; (2) applications of the latest SNCR technologies in large-scale CFB boilers, such as new urea-based ammonia-releasing reduction agents from ERC Technik, Selective Cooling and TWIN-NO_x® technologies from M&S, acoustic gas temperature measurement and advanced control systems; and (3) more comprehensive measurements in dilute phase zone to verify their relationship with gas distribution at the corresponding SNCR inlet, thus to predict the level of original NO_x distribution and the subsequent SNCR process.

Author Contributions: Conceptualization, X.L. and J.Y.; investigation, J.Y., X.Z. and X.F.; methodology, X.L. and J.Y.; writing—original draft preparation, J.Y.; writing—review and editing, C.Z., Q.L. and J.W.; and validation, S.L. and C.Z. All authors have read and agreed to the published version of the manuscript.

Institutional Review Board Statement: Not applicable.

Informed Consent Statement: Not applicable.

Data Availability Statement: No new data were created or analyzed in this study. Data sharing is not applicable to this article.

Conflicts of Interest: The authors declare no conflict of interest.

References

1. Blaszczuk, A.; Nowak, W. Heat transfer behavior inside a furnace chamber of large-scale supercritical CFB reactor. *Int. J. Heat Mass Tran.* **2015**, *87*, 464–480. [CrossRef]

2. Yue, G.X.; Cai, R.X.; Lyu, J.F.; Zhang, H. From a CFB reactor to a CFB boiler—The review of R&D progress of CFB coal combustion technology in China. *Powder Technol.* **2017**, *316*, 18–28.

3. Blaszczuk, A.; Pogorzelec, M.; Shimizu, T. Heat transfer characteristics in a large-scale bubbling fluidized bed with immersed horizontal tube bundles. *Energy* **2018**, *162*, 10–19. [CrossRef]

4. Chen, H.W.; Song, Y.F.; Yang, S.; Xin, Y. Prediction of particle circulation rate in an internally circulating fluidized bed with a central draft tube. *Powder Technol.* **2021**, *380*, 497–505. [CrossRef]

5. Ji, J.Q.; Cheng, L.M.; Wei, Y.J.; Wang, J.F.; Gao, X.Y.; Fang, M.X.; Wang, Q.H. Predictions of NO_x/N_2O emissions from an ultra-supercritical CFB boiler using a 2-D comprehensive CFD combustion model. *Particuology* **2020**, *49*, 77–87. [CrossRef]

6. Blaszczuk, A.; Nowak, W.; Jagodzik, S. Effects of operating conditions on $deNO_x$ system efficiency in supercritical circulating fluidized bed boiler. *J. Power Technol.* **2013**, *93*(1), 1–8.

7. Ke, X.W.; Li, D.F.; Li, Y.R.; Jiang, L.; Cai, R.X.; Lyu, J.F.; Yang, H.R.; Zhang, M.; Jeon, C.H. 1-Dimensional modelling of in-situ desulphurization performance of a 550 MWe ultra-supercritical CFB boiler. *Fuel* **2021**, *290*, 120088. [CrossRef]

8. Li, J.J.; Yang, H.R.; Wu, Y.X.; Lv, J.F.; Yue, G.X. Effects of the updated national emission regulation in China on circulating fluidized bed boilers and the solutions to meet them. *Environ. Sci. Technol.* **2013**, *47*, 6681–6687. [CrossRef]

9. Ke, X.W.; Cai, R.X.; Zhang, M.; Miao, M.; Lyu, J.F.; Yang, H.R. Application of ultra-low NOx emission control for CFB boilers based on theoretical analysis and industrial practices. *Fuel Process. Technol.* **2018**, *181*, 252–258. [CrossRef]

10. *The Upgrade and Retrofitting Action Plan of Energy Saving and Emission Reduction for Coal-Fired Power Plants*; National Development and Reform Commission: Beijing, China, 2014.

11. Sirisomboon, K.; Charernporn, P. Effects of air staging on emission characteristics in a conical fluidized-bed combustor firing with sunflower shells. *J. Energy Inst.* **2017**, *90*, 316–323. [CrossRef]

12. Misiulia, D.; Antonyuk, S.; Andersson, A.G.; Lundstrom, T.S. High-efficiency industrial cyclone separator: A CFD study. *Powder Technol.* **2020**, *364*, 943–953. [CrossRef]

13. Liu, X.M.; Yang, H.R.; Lyu, J.F. Optimization of fluidization state of a circulating fluidized bed boiler for economical operation. *Energies* **2020**, *13*, 376. [CrossRef]

14. Fang, D.D.; Zhang, L.H.; Duan, F.; Chyang, C.S.; Wang, Y.C. Combustion and pollutant emissions characteristics of Camellia oleifera shells in a vortexing fluidized-bed combustor. *J. Energy Inst.* **2020**, *93*, 739–751. [CrossRef]

15. Ljungdahl, B.; Larfeldt, J. Optimised NH_3 injection in CFB boilers. *Powder Technol.* **2001**, *120*, 55–62. [CrossRef]

16. Kang, Z.Z.; Yuan, Q.X.; Zhao, L.Z.; Dai, Y.K.; Sun, B.M.; Wang, T. Study of the performance, simplification and characteristics of SNCR de-NO_x in large-scale cyclone separator. *Appl. Therm. Eng.* **2017**, *123*, 635–645. [CrossRef]

17. Yao, T.; Duan, Y.F.; Yang, Z.Z.; Li, Y.; Wang, L.W.; Zhu, C.; Zhou, Q.; Zhang, J.; She, M.; Liu, M. Experimental characterization of enhanced SNCR process with carbonaceous gas additives. *Chemosphere* **2017**, *177*, 149–156. [CrossRef] [PubMed]

18. Rahman, Z.; Wang, X.B.; Zhang, J.Y.; Baleta, J.; Vujanovic, M.; Tan, H.Z. Kinetic study and optimization on SNCR process in pressurized oxy-combustion. *J. Energy Inst.* **2021**, *94*, 263–271. [CrossRef]

19. Świeboda, T.; Krzyżyńska, R.; Bryszewska-Mazurek, A.; Mazurek, W.; Czapliński, T.; Przygoda, A. Advanced approach to modeling of pulverized coal boilers for SNCR process optimization—Review and recommendations. *Int. J. Thermofluid.* **2020**, *7–8*, 100051. [CrossRef]

20. Yan, J.; Lu, X.F.; Wang, Q.H.; Kang, Y.H.; Li, J.B.; Zhou, J.; Zhang, Y.; Lv, Z.; Sicong, S. Experimental and numerical study on air flow uniformity in the isobaric windbox of a 600 MW supercritical CFB boiler. *Appl. Therm. Eng.* **2017**, *122*, 311–321. [CrossRef]

21. Zheng, W.J.; Zhang, M.; Zhang, Y.; Lyu, J.F.; Yang, H.R. The effect of the secondary air injection on the gas–solid flow characteristics in the circulating fluidized bed. *Chem. Eng. Res. Des.* **2019**, *141*, 220–228. [CrossRef]

22. Yan, J.; Lu, X.F.; Zheng, X.; Xue, R.; Lei, X.J.; Fan, X.C.; Liu, S.R. Experimental investigations on lateral dispersion coefficients of fuel particles in large-scale circulating fluidized bed boilers with different coal feeding modes. *Energies* **2020**, *13*, 6336. [CrossRef]

23. Ma, S.X.; Chang, W.M.; Zhang, J.C.; Luo, D.L. Optimizing calculation of particle size distribution of feeding coal for circulating fluidized bed boiler. *Appl. Therm. Eng.* **2015**, *87*, 463–470. [CrossRef]

24. Yan, J.; Lu, X.F.; Song, Y.F.; Zheng, X.; Lei, X.J.; Liu, Z.; Fan, X.C.; Liu, C.C. A comprehensive understanding of the non-uniform characteristics and regulation mechanism of six external loops in a 600 MW supercritical CFB boiler. *Energy* **2021**, 120032, in press. [CrossRef]

25. Yuan, Z.W.; Meng, L.; Gu, X.B.; Bai, Y.Y.; Cui, H.M.; Jiang, C.Y. Prediction of NO_x emissions for coal-fired power plants with stacked-generalization ensemble method. *Fuel* **2021**, *289*, 119748. [CrossRef]

26. Zhou, G.Y.; Jin, B.S. Ammonia injection method for SCR based on non-uniform inlet condition. *J. Huazhong Univ. Sci. Tech.* **2016**, *44*, 121–126. [CrossRef]

27. Liu, G.F.; Zhang, Y.; Shen, D.K.; Yuan, B.; Li, R.; Sun, Y. Anticipatory NH3 injection control for SCR system based on the prediction of the inlet NO_x concentration. *J. Energy Inst.* **2021**, *94*, 167–175. [CrossRef]

28. Niklasson, F.; Johnsson, F.; Leckner, B. Locao air ratio measured by zirconia cell in a circulating fluidised bed furnace. *Chem. Eng. J.* **2003**, *96*, 145–155. [CrossRef]

29. Hartge, E.-U.; Fehr, M.; Werther, J.; Ochodek, T.; Noskievic, P.; Krzin, I.; Kallner, P.; Gadowski, J. Gas concentration measurements in the combustion chamber of the 235 MWe circulating fluidized bed boiler Turow no 3. In Proceedings of the 18th International Conference on Fluidized Bed Combustion, Toronto, ON, Canada, 22–25 May 2005.

30. Yan, J.; Lu, X.F; Wang, Q.H.; Kang, Y.H.; Li, J.B.; Xu, Z.; Lei, X.; Zheng, X.; Fan, X.; Liu, Z. Study on the influence of secondary air on the distributions of flue gas composition at the lower part of a 600 MW supercritical CFB boiler. *Fuel Process. Technol.* **2019**, *196*, 106035. [CrossRef]

31. Werther, J.; Hartge, E.-U.; Ratschow, L.; Wischnewski, R. Simulation-supported measurements in large circulating fluidized bed combustors. *Particuology* **2009**, *7*, 324–331. [CrossRef]

32. Lu, J.Y.; Lu, X.F.; He, H.H.; Wang, H.; Gan, L.; Zhao, P.; Tang, X.N. Combustion characteristics of the external circulation loop on Baima's 300 MWe circulating fluidized bed boiler. *Energy Fuel* **2011**, *25*, 3456–3464. [CrossRef]

33. Yan, J.; Lu, X.F.; Xue, R.; Lu, J.Y.; Zheng, Y.; Zhang, Y.; Liu, Z. Validation and application of CPFD model in simulating gas-solid flow and combustion of a supercritical CFB boiler with improved inlet boundary conditions. *Fuel Process. Technol.* **2020**, *208*, 106512. [CrossRef]

34. Vodička, M.; Hrdlička, J.; Skopec, P. Experimental study of the NO_x reduction through the staged oxygen supply in the oxy-fuel combustion in a 30 kW_{th} bubbling fluidized bed. *Fuel* **2021**, *286*, 119343. [CrossRef]

35. Song, G.L.; Yang, X.T.; Yang, Z.; Xiao, Y. Experimental study on ultra-low initial NO_x emission characteristics of Shenmu coal and char in a high temperature CFB with post-combustion. *J. Energy Inst.* **2021**, *94*, 310–318. [CrossRef]

36. Guo, Q.; Wang, Q.H.; Lu, X.F.; Li, J.B.; Xu, J. Numerical study on gas flow characteristics in three parallel separators of a large-scale CFB boiler. *Proc. CSEE* **2019**, *39*, 3851–3858.

37. Wang, W. *Numerical Simulation of the SNCR Denitration Process in a Circulating Fluidized Bed*; Southeast University: Nanjing, China, 2016.